Journal Pre-proof

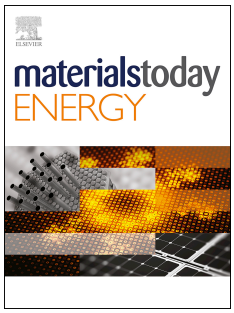

Pathway of *in situ* Polymerization of 1,3-dioxolane in $LiPF_6$ Electrolyte on Li Metal Anode

Miao Xie, Yu Wu, Yue Liu, Peiping Yu, Ran Jia, William A. Goddard, III, Tao Cheng

PII: S2468-6069(21)00095-2

DOI: https://doi.org/10.1016/j.mtener.2021.100730

Reference: MTENER 100730

To appear in: *Materials Today Energy*

Received Date: 4 March 2021

Revised Date: 18 March 2021

Accepted Date: 20 March 2021

Please cite this article as: M. Xie, Y. Wu, Y. Liu, P. Yu, R. Jia, W.A Goddard III., T. Cheng, Pathway of *in situ* Polymerization of 1,3-dioxolane in $LiPF_6$ Electrolyte on Li Metal Anode, *Materials Today Energy*, https://doi.org/10.1016/j.mtener.2021.100730.

Credit Author Statement

Xie Miao, Goddard III William A and Cheng Tao: Conceptualization

Xie Miao, Wu Yu, Liu Yue, Peiping: Investigation

All authors: Writing - Original Draft

All authors: Writing - Review & Editing

Goddard III William A and Cheng Tao: Supervision

Pathway of *in situ* Polymerization of 1,3-dioxolane in $LiPF_6$ Electrolyte on Li Metal Anode

Miao Xie,[a] Yu Wu,[a] Yue Liu,[a] Peiping Yu,[a] Ran Jia,[b] William A Goddard III[c,*], and Tao Cheng [a,*]

[a] *Institute of Functional Nano and Soft Materials (FUNSOM), Soochow University, Suzhou 215123, China.*

[b] *Institute of Theoretical Chemistry, Jilin University, Changchun 130023, China.*

[c] *Materials and Process Simulation Center, California Institute of Technology, Pasadena, California 91125, USA*

[*]Corresponding author.

E-mail address:

tcheng@suda.edu.cn (T. Cheng)

wag@caltech.edu (WAG)

ABSTRACT

Although the lithium metal battery has been considered to be one of the most promising candidates to facilitate high-density energy storage, the practical applications of lithium metal anodes are significantly hindered by its high reactivity. Electrolytes based on 1,3-dioxolane (DOL) have been demonstrated to be one of the most effective electrolytes that can suppress side reactions, but the underlying mechanism is still far from clear. In this work, we carried out multi-scale simulations that combine density functional theory (DFT) and reactive force field (ReaxFF) to investigate the initial reactions of 1.0 M $LiPF_6$ salt in DOL with Li metal anode. Our simulation results reveal that PF_6^- anions can either fully decompose via reduction reaction when they directly in contact with Li anode or convert to PF_5 when they stay in bulk. While the decomposition products (F^- and P_x^-) contribute to the formation of the inorganic part of the solid electrolyte interphase (SEI), the latter PF_5 can serve as an initiator of the polymerization of DOL. Such polymerization of the electrolyte provides an unexpected protective effect that resembles the polymer electrolyte but is formed in situ. The most kinetically favorable polymerization pathway is then distinguished from hybrid functional DFT calculations, which confirms that PF_5 plays an important role in activating the DOL ring for further polymerization. The insights revealed from this work should be of help to expedite the rational design of electrolytes that provide protective SEI to stabilize Li anode.

Keywords: Battery; SEI; Computational Modeling; DFT; Electrolyte

1. Introduction

Nowadays, energy utilization has gradually shifted from traditional fossil energy sources to low carbon and renewable energy to achieve the goal of sustainable development. Hence, there is an urgent need for new large-scale battery technologies with high capacity, high energy density, and reliable efficiency [1-3]. Although the capacity of lithium-ion batteries (LIBs) taking carbon materials as the anode is approaching its theoretical capacity (372 mA $h \cdot g^{-1}$), the energy density provided by carbon-host is still far from meeting the requirement of the increasingly high demand of chargeable portable devices, electric vehicles, and large-scale grid energy storage [4,5]. Lithium metal anode has the highest theoretical capacity (3860 mA $h \cdot g^{-1}$) and the most negative electrochemical potential, 3.04 V, when referring to a standard hydrogen electrode (SHE) [6,7]. As a result, lithium metal batteries (LMBs) taking lithium metal anode are one of the most promising candidates for new generations of high energy density storage devices.

The high activity of lithium metal leading to unexpected side reactions poses significant impedance in the development of LMBs. Meanwhile, the uncontrolled growth of lithium dendrite will cause extreme side reactions with organic liquid electrolyte (LE) and lead to safety problems. Lithium dendrite, on the one hand, punctures the diaphragm and spreads to the positive electrode, resulting in electrical contact and short circuit within the battery, and causes fire and explosion. On the other hand, lithium dendrite has high reactivity and

absorbs electrolyte and active lithium, resulting in constant thickening of the solid electrolyte interphase (SEI), resulting in lower Coulomb efficiency and a shorter life cycle.[7-13] Simultaneously, electrochemical losses due to uneven stripping of lithium metal during discharge would further lead to the formation of dead lithium, thereby reducing the available active lithium and thus reducing the performance of Coulomb. To solve the above issues, researchers have used a number of techniques to improve the efficiency of metal lithium batteries, such as the use of alloy anode [14], electrolyte structure optimization [14-16], solid electrolyte development [17], artificial SEI film [18-20], 3D lithium deposition framework [21,22], etc. However, it is still challenging to realize the commercial operation of metal lithium batteries.

Optimization and production of electrolyte systems are important among these techniques to improve the efficiency of lithium metal anode. For example, electrolyte regulation is currently one of the most powerful and convenient ways of promoting long-term cycling efficiency and inhibiting dendrite formation. Changes in the composition, additives, and concentrations of the electrolyte can influence the action of lithium deposition and the decomposition of the organic species and then influence the composition and structure of the SEI [23-25]. In order to increase the performance of the Coulomb efficiency, the understanding of the SEI process between the electrolyte and the lithium metal anode is therefore crucial to solving problems such as lithium metal dendrite and the corrosion of the lithium metal anode. Unfortunately, many key

problems can not be fundamentally solved because the related reaction mechanism of lithium metal anode is not completely clear, such as the interaction with electrolyte, lithium deposition, and so on.

A significant amount of experimental results show that the electrolyte, such as DOL, likely polymerizes during SEI formation. Effective control of the polymerization reaction can substantially improve the stability of SEI. For example, in the research of Zhao et al., ultra-stable SEI was achieved by in-situ producing polymer electrolytes with the help of salt [26]. However, the understanding of the mechanism of surface polymerization is still far from clear. Phenomenon models have been proposed but of limited help due to lack of details [27]. Our work has combined multiple multi-scale simulation methods to investigate the possible reaction paths in detail, which provides a theoretical basis for further improvement of SEI stability.

Employing the atomic-scale simulation method, it can predict material properties, simulate the reaction process, and become one of the effective tools for screening materials and revealing reaction mechanisms. In this work, we apply a multi-scale simulation method to simulate the degradation process of 1.0 Mol L-1 $LiPF_6$ salt in 1,3-dioxolane (DOL) electrolyte on a lithium metal electrode. As a kind of low molecular weight polyether, DOL has the satisfactory ability to form stable interphase when in contact with lithium metal anode, which can make the anode have a high level of reversibility.[26,28] Moreover, $LiPF_6$ salts, as the most commonly used electrolyte salts, are also

widely used in lithium metal batteries. The combination of this electrolyte is very representative, and the electrolyte has achieved satisfactory performance in practical application. Hence, it is of great significance to investigate the mechanism of the reaction of electrolyte with lithium metal electrode to form SEI film. We hope that this research work can deepen the understanding of the SEI formation mechanism and contribute to the design of a new electrolyte.

2. Computational details

In previous work, we used the QM-MD and ReaxFF-MD hybrid scheme to study the reaction process of electrolyte at lithium metal anode surface and obtained accurate results consistent with the experiment [29,30]. In the quantum mechanics (QM) molecular dynamics (MD) simulation, we employed 1 $LiPF_6$ and 13 DOL to simulate the $LiPF_6$-DOL electrolyte, which represents a 1M concentration of Li-salts in the electrolyte. The Li anode was simulated by employing a 3 by 3 by 6 Li (100) surface with 54 Li atoms, where the bottom 2 Li atom layers were fixed during the simulation. The vacuum between the anode and its periodic image is set according to the experimental density of the electrolyte (a density of 1.06 g/cm^3). Then, the components of the electrolyte were randomly inserted into the vacuum, forming the electrolyte/anode half-cell with two explicit electrolyte/anode interfaces. The final simulation periodic cell was 10.47 × 10.47 × 26.73 Å. We then carried out QM optimization followed by MD equilibration and 3 ps MD NVT simulation to investigate the initial reaction. Significant initial chemical reactions were observed in 3 ps of QM

molecular dynamics (QM-MD) simulations. To further investigate the interaction between DOL and PF_5 molecule (PF_6^- decomposition product), we constructed a model containing 9 DOL molecules and 3 PF_5 molecules using a cell parameter of a = b = c = 11.4 Å. Then, we carried out QM optimization followed by MD equilibration and 5 ps NVT simulation.

All the QM-MD calculations were carried out using the VASP software (version 5.4.4) [31,32]. We used the Perdew, Burke, and Ernzerhof (PBE) [33] flavor of density functional theory (DFT) with the post-stage DFT-D3 method to correct for London dispersion (van der Waals attraction) with Becke-Johnson damping.[34] The projector augmented wave (PAW) method was used to account for core-valence interactions.[35,36] The kinetic energy cutoff for plane wave expansions was set to 400 eV, and reciprocal space was sampled by the Γ-centered Monkhorst-Pack scheme with a grid of 1 × 1 × 1. A conjugate gradient algorithm with an energy criterion of 1×10^{-5} eV was used for atomic convergence, and the forces were guaranteed to be smaller than 0.01 eV $Å^{-1}$. The time step was set 1 fs.

The ReaxFF simulations used the Large-scale Atomic/Molecular Massively Parallel Simulator (LAMMPS 2018) software. The time step was set to 0.25 fs. We started with the ReaxFF parameters developed by Islam et al., which we are using training data from accurate QM calculations combined with the Monte Carlo simulated annealing (MC) force field optimization method. The ReaxFF reactive force field uses bond order-dependence to describe bond

breaking. The parameters were optimized by fitting QM but including some experimental results. ReaxFF bond orders (BO_{ij}) are calculated instantaneously. They contain sigma, pi, and double-pi bonds, as in Eq. (1).

$$BO'_{ij} = BO^{\sigma}_{ij} + BO^{\pi}_{ij} + BO^{\pi\pi}_{ij}$$
$$= \exp[p_{bo1} \cdot (\frac{r_{ij}}{r_0^{\sigma}})^{p_{bo2}}] + \exp[p_{bo3} \cdot (\frac{r_{ij}}{r_0^{\pi}})^{p_{bo4}}] + \exp[p_{bo5} \cdot (\frac{r_{ij}}{r_0^{\pi\pi}})^{p_{bo6}}] \quad \text{..... (1)}$$

During the force field optimization procedure, the error objective function was expressed as deviations between QM and ReaxFF energies and forces as in Eq. (2). Here $x_{i,}$ and $x_{i,\,ReaxFF}$ are the corresponding values for QM and ReaxFF results, σ_i is the weight parameter adjusted based on the accuracy in the training data.

$$Error = \sum_{i=1}^{n} [\frac{x_{i,QM} - x_{i,\mathrm{Re}axFF}}{\sigma_i}]^2 \quad \text{..... (2)}$$

Since finding the global minimum error function is essential to guarantee the accuracy of ReaxFF results, we use Monte Carlo Simulated Annealing (MC) to optimize ReaxFF force field parameters [37,38].

To study the mechanism of DOL molecular polymerization, molecular geometries of all models were optimized without constraints by density functional theory (DFT) calculations using the B3LYP functional [39] with 6-31G(d) basis set for all atoms. To take the dispersion interactions into account, we consider the DFT-D3 dispersion correction [34]. The vibrational

frequencies were computed at the same level to identify all of the stationary points as transition states (one imaginary frequency) or as minima (zero imaginary frequencies) and evaluate its zero-point vibrational energy (ZPVE) and thermal corrections at 298 K. All transition states that these structures indeed connect two relevant minima were confirmed by intrinsic reaction coordinates (IRC) calculation [40,41]. In terms of considering solvent effects, the single-point energy calculations were performed at the level of B3LYP with the 6-311+G(d,p) basis set for all atoms. Besides, solvent effects were considered using the continuum solvent model SMD [42] for 1,3-dioxolane (DOL, the dielectric constant is 7.13), which was used as the solvent in this experimental study. The Gibbs free energy for each species is taken as the sum of the thermal correction to free energies in the gas phase and the single-point energy in solution. All calculations were performed with the Gaussian 16 suite of programs (Revision A.03) [43].

3. Results and discussion

3.1 QM-MD result of $LiPF_6$-DOL system

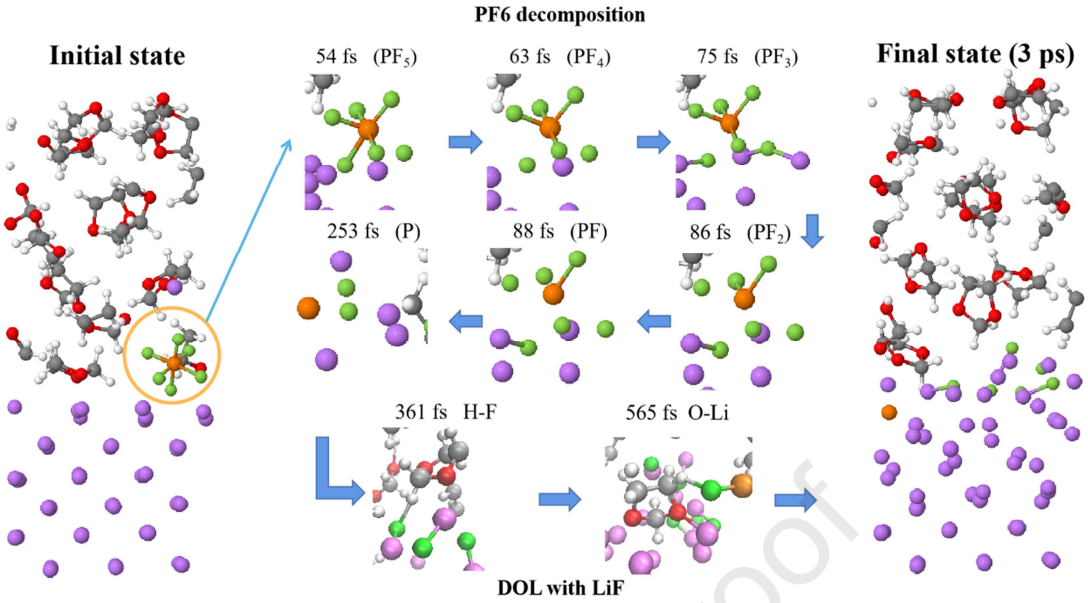

Fig. 1. The reactive snapshots of the decomposition of PF_6^- and DOL and LiF interaction after 3 ps QM-MD simulation of the $LiPF_6$-DOL system. Color code: lithium, purple; oxygen, red; carbon, gray; fluorine, green; hydrogen, white.

Generally, the SEI film mainly contains two parts of the inorganic and organic layer during the charge-discharge cycle of lithium metal battery, which separates electrolyte and electrode to prevent further reaction [44,45]. In order to explore the initial mechanism for degradative reduction of electrolytes on lithium metal anode system, we analyze MD trajectories during QM-MD simulations. In the electrolyte of $LiPF_6$–DOL, as shown in Fig. 1, we observed the following reactions in QM-MD simulation: At the beginning, the main process is the lithium diffusion process within the 55 fs. PF_6^- react with Li atom to produce $PF_5\cdot$ and LiF until 57 fs. Then $PF_5\cdot$ continues to decompose with Li atoms to produce LiF and PF_4 at 63 fs. At 75 fs $PF_4^{\cdot}$ continue to remove F- ions

to form product $PF_3\cdot$ and LiF. We observe that $PF_3\cdot$ can still react with Li to generate $PF_2\cdot$ and LiF at 86 fs. The $PF_2\cdot$ dissociates an F- to form $PF\cdot$ and LiF at 88 fs. Lastly, $PF\cdot$ is completely decomposed into LiF and $P^{\cdot}$ radical at 253 fs. The LiF as one of the SEI components also has some unique properties: [46,47] high mechanical strength [48], low solubility[49], and low lithium-ion diffusion barrier [50]. It suggests that LiF may promote a more uniform lithium-ion distribution and inhibit disordered lithium dendrite generation [51]. Complete decomposition of PF_6^- consumes 6 Li atoms, very efficiently in promoting the formation of protective SEI. The overall reaction is as follows:

$$LiPF_6 + 8\,Li^0 \rightarrow Li_3P + 6\,LiF \qquad (3)$$

Interestingly, we found some structures in the QM-MD trajectory, which may be the initial stage of DOL polymerization in situ. The O atoms of DOL molecules can bind to the Li^+ of the LiF to form Li-O bonds. Moreover, the H atoms of DOL molecules can also combine with the F^- of the LiF to form F-H. These sites can make DOL directly and stably connected to the inorganic LiF layer. Once the DOL molecules on the LiF layer react with the initiator, a good SEI of the inner inorganic LiF and the outer organic polymer can be formed, which can better protect the lithium metal anode. At 361 fs, we observed DOL molecules linked to the LiF through the F-H bond. Then another DOL molecule with a LiF structure connected by Li-O bonds was found at 565 fs. Overall, when the PF_6^- decomposition is generated LiF, these structures appear many

times in the simulation of 3 ps. Due to the limitation of QM-MD simulation time length, we did not directly observe the polymerization of DOL molecules.

3.2 ReaxFF MD result of $LiPF_6$-DOL system

Nevertheless, limited by computational cost and time scale, we cannot simulate the SEI formation process in lithium metal batteries by QM-MD. Hence, we use the ReaxFF reactive force field approach to extend the simulation time scale and wish to observe more important information about the generation of SEI processes. For this reason, the ReaxFF reactive force field simulations were conducted for 95 ps.

At first, the degradation reaction initiates by breaking the P-F bond of PF_6^-, forming PF_4 and LiF at around 5.0 ps is given in Fig. 2. And these results are consistent with that of QMMD simulation. When about 60 ps, it was observed that the C-O bond of the DOL molecule broke, and the bond length changed from 1.449 Å to 1.745 Å, resulting in $OCH_2OCH_2CH_2$ formation. Then about 90 ps, the O-C bond of $OCH_2OCH_2CH_2$ were connected to form DOL molecules. Lastly, the stable products are LiF salts, $PF_4\cdot$ (PF_6^- decomposition product), and DOL molecules during the 95 ps simulation.

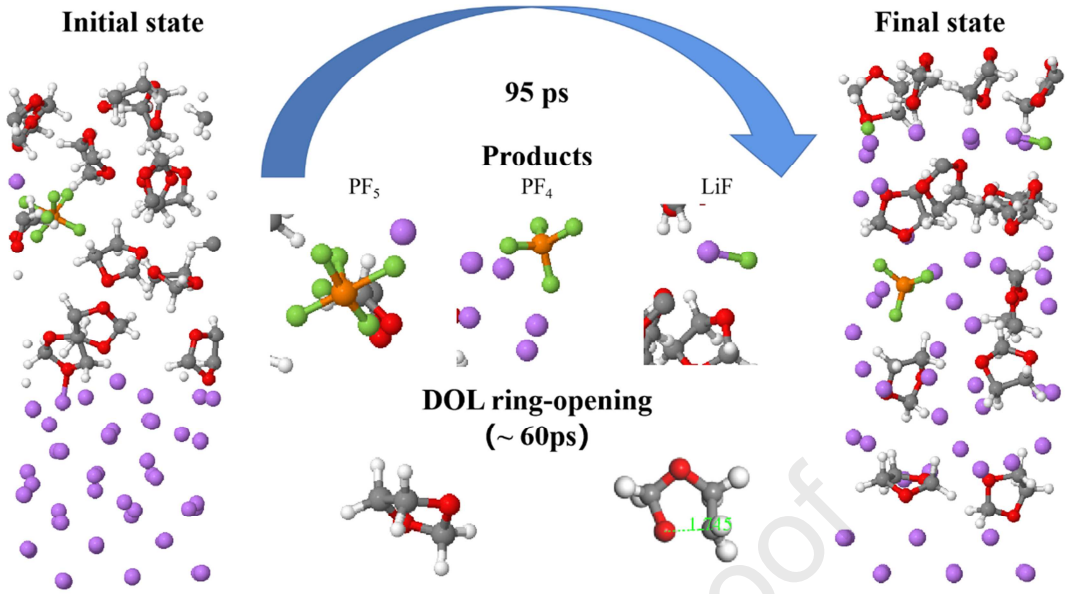

Fig. 2 Snapshots of $LiPF_6$ and DOL decomposition obtained from the ReaxFF reactive force field simulations for the $LiPF_6$-DOL system. Color code as in Fig. 1.

3.3 QM-MD result of PF_5-DOL system

In our work, we suspect that PF_6^- also serves a crucial role in promoting the polymerization of DOL. In our simulation, we noticed that PF_6^- decomposed into F- while leaving PF_5 with a radical character in the electrolyte. To investigate the effect of the PF_5 radical, we simulated with 3 PF_5 radicals into the 9 DOL solvent, and the simulation time scale was 5 ps.

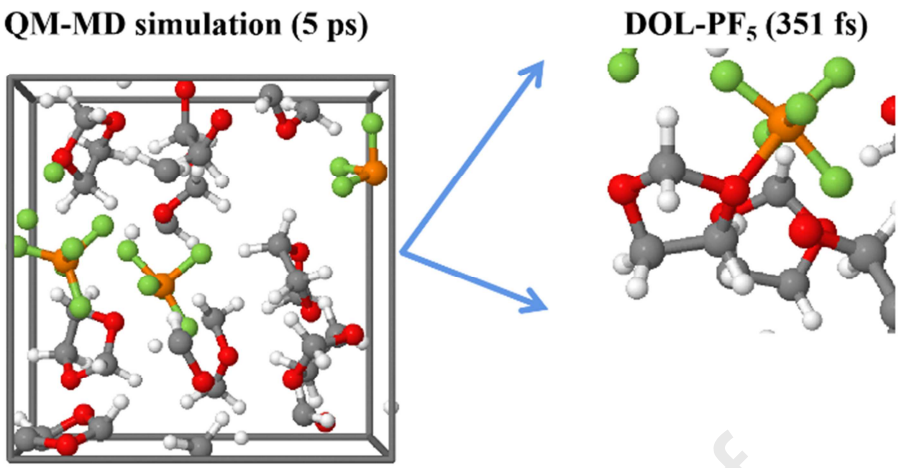

Fig. 3 The structure of DOL-PF5 obtained from 3 ps QM-MD simulation of the PF5-DOL system.

In Fig. 3, we observed that DOL molecules were linked to the PF_5 by generating P-O bonds after 351 fs. The stable PF_5 structure is triangular bipyramids, and when the DOL molecules are close to the PF_5 to form a P-O bond, the PF_5 structure becomes octahedral. Then, the rest of the DOL molecules moved closer to the DOL-PF_5 system. Although no DOL ring opening and polymerization occurred in 5 ps, the initial reaction state of DOL polymerization has gradually become clear.

3.4 DOL with PF_5 polymerization mechanisms

In order to study the reaction of DOL molecular polymerization, we propose the following reaction mechanism: PF_6^- reacts with Li atoms to remove one F^- ion to form LiF and PF_5, in which the product PF_5 can be used as an initiator for polymerization. Next, the lone pair of electrons of O atoms in DOL molecules combine with P atoms of the PF_5 to form DOL-PF_5. The C-O bond of

the DOL molecule in the DOL-PF_5 system is activated, and the other DOL molecules attack the C atom, and then the ring-opening reaction occurs to form a DOL-L-PF_5. The C-O bonds of the unopened part of the DOL molecule in the DOL-L-PF_5 system continue to be activated, and the C atoms can combine with other DOL molecules to form 2DOL-L-PF_5. The 2DOL-L-PF_5 system continues to undergo ring-opening reactions to generate DOL-L_2-PF_5. Finally, DOL molecular ring-opening reactions occur continuously in this way, resulting in the formation of polymers.

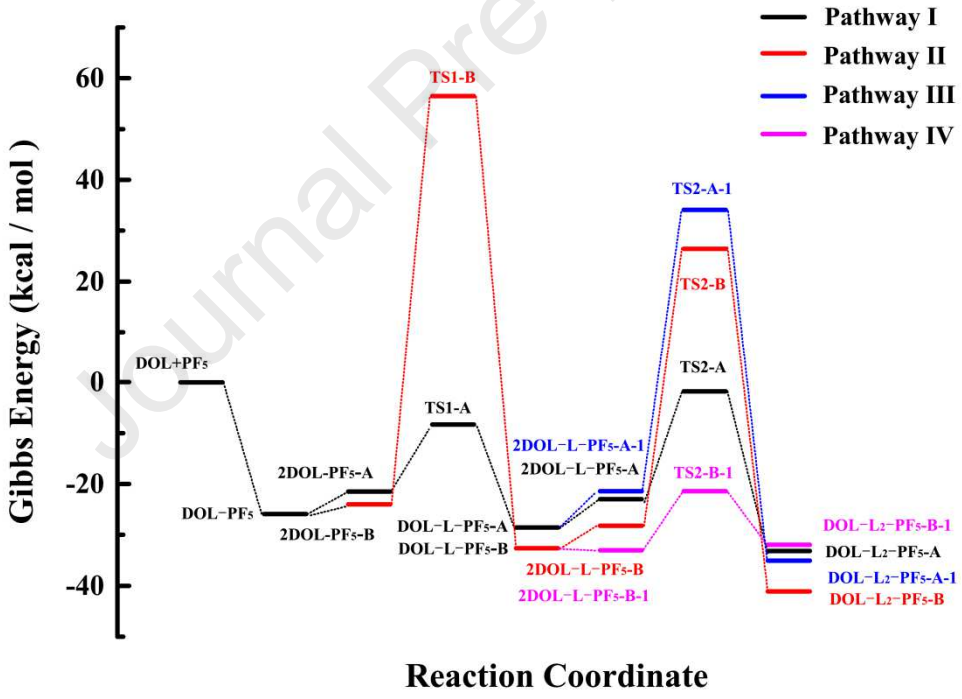

Fig. 4 Gibbs energy profile calculated for the DOL polymerization. The calculated relative free energies are given in kcal/mol.

$$LiPF6 \longrightarrow LiF + PF_5$$

Pathway I

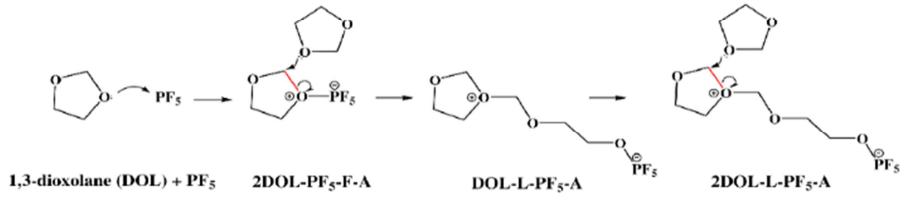

1,3-dioxolane (DOL) + PF_5 2DOL-PF_5-F-A DOL-L-PF_5-A 2DOL-L-PF_5-A

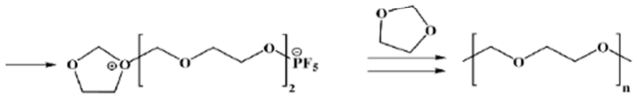

DOL-L_2-PF_5-A Polymer

Pathway II

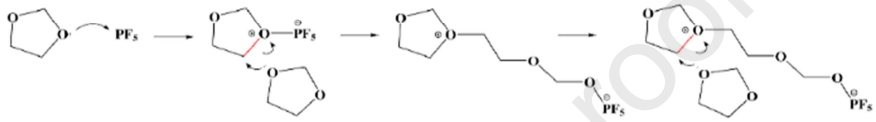

1,3-dioxolane (DOL) + PF_5 DOL-PF_5-B DOL-L-PF_5-B 2DOL-L-PF_5-B

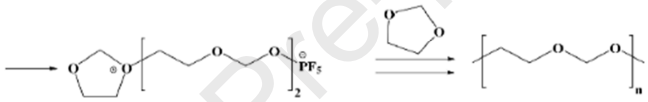

DOL-L_2-PF_5-B Polymer

Pathway III

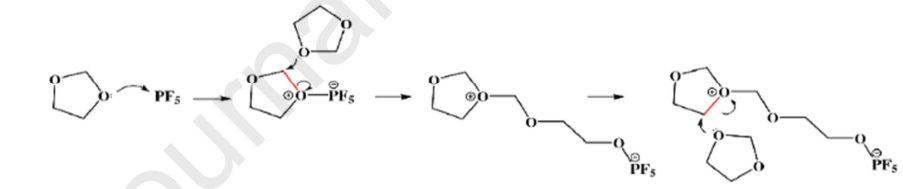

1,3-dioxolane (DOL) + PF_5 2DOL-PF_5-A DOL-L-PF_5-A 2DOL-L-PF_5-A-1

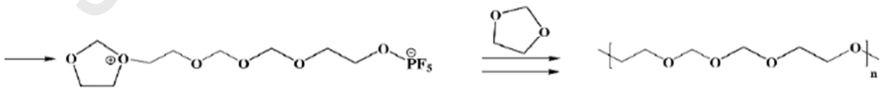

DOL-L_2-PF_5-A-1 Polymer

Pathway IV

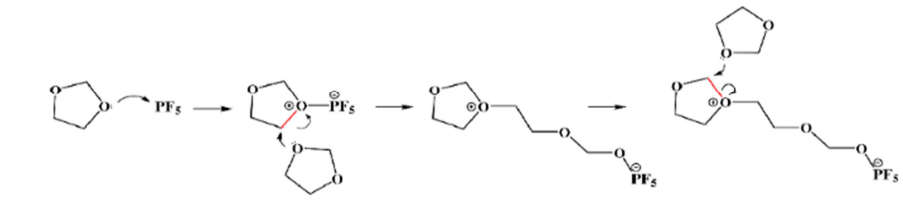

1,3-dioxolane (DOL) + PF_5 2DOL-PF_5-B DOL-L-PF_5-B 2DOL-L-PF_5-B-1

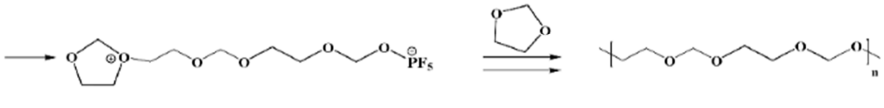

DOL-L_2-PF_5-B-1 Polymer

Scheme 1. Four possible reaction mechanisms for DOL polymerization.

There are four possible reaction mechanisms for DOL polymerization are shown in Scheme 1. Based on the above reaction path, we calculated the free energy of the polymerization reaction listed in Fig. 4 and Table 1. The free energy of the interaction between DOL and PF_5 as initiator is -25.91 Kcal/mol (-1.124 eV), which indicates that PF_5 and DOL can form stable product DOL-PF_5. Next, the other DOL molecule has two reaction pathways: one is bound to the C atom between the two O atoms of the DOL molecule, the other is the interaction with C atoms in the middle of the O atom and C atom in the DOL molecule. Other DOL combines with DOL-PF_5 to generate 2DOL-PF_5-A and 2DOL-PF_5-B, respectively, and their energy is very close. In pathway I, through the transition state TS_1-A, a ring-opening reaction occurs to generate DOL-L-PF_5-A. The energy barrier for this reaction pathway is 13.14 kcal/mol (TS_1-A a relative to reactant 2DOL-PF_5-A). Moreover, in the other pathway II, the O-C bond of intermediate 2DOL-PF_5-B broke via transition state TS_1-B (80.48 kcal/mol) to form DOL-L-PF_5-B. Comparing two pathways, it is found that TS_1-A is much lower than TS_1-B by 67.34 kcal/mol, suggesting that pathway I giving the DOL-L-PF_5-A is more favorable than the latter one generating the DOL-L-PF_5-B.

Then we find that there are two reaction pathways from intermediate DOL-L-PF_5-A. In the same way, as mentioned above, DOL continues to combine with DOL-L-PF_5-A, the reaction pathway can be divided into pathway

I and pathway III. The same trends have been obtained for the second DOL

Table 1 Calculated Gibbs free energy of the polymerized DOL reaction at the level of B3LYP with the 6-311+G(d,p) basis set.

DOL Polymerization Reaction		ΔG	
		eV	Kcal/mol
Pathway I	DOL + PF_5 → DOL-PF_5	-1.12	-25.91
	DOL + DOL-PF_5 → 2DOL-PF_5-A	0.19	4.44
	2DOL-PF_5-A → TS_1-A	0.57	13.16
	TS_1-A → DOL-L-PF_5-A	-0.88	-20.23
	DOL + DOL-L-PF_5-A→ 2DOL-L-PF_5-A	0.24	5.59
	2DOL-L-PF_5-A → TS_2-A	0.92	21.19
	TS_2-A → DOL-L_2-PF_5-A	-1.36	-31.39
Pathway II	DOL + PF_5 → DOL-PF_5	-1.12	-25.91
	DOL + DOL-PF_5 → 2DOL-PF_5-B	0.08	1.92
	2DOL-PF_5-B → TS_1-B	3.49	80.48
	TS_1-B → DOL-L-PF_5-B	-3.86	-89.07
	DOL + DOL-L-PF_5-B→ 2DOL-L-PF_5-B	0.19	4.40
	2DOL-L-PF_5-B → TS_2-B	2.37	54.59
	TS_2-B → DOL-L_2-PF_5-B	-2.93	-67.51
Pathway III	DOL + PF_5 → DOL-PF_5	-1.12	-25.91
	DOL + DOL-PF_5 → 2DOL-PF_5-A-1	0.19	4.44
	2DOL-PF_5-A-1 → TS_1-A-1	0.57	13.16
	TS_1-A-1 → DOL-L-PF_5-A-1	-0.88	-20.23
	DOL + DOL-L-PF_5-A-1→ 2DOL-L-PF_5-A-1	0.31	7.17
	2DOL-L-PF_5-A-1 → TS_2-A-1	2.41	55.48
	TS_2-A-1 → DOL-L_2-PF_5-A-1	-3.00	-69.15
Pathway IV	DOL + PF_5 → DOL-PF_5	-1.12	-25.91
	DOL + DOL-PF_5 → 2DOL-PF_5-B-1	0.08	1.92

2DOL-PF_5-B-1 → TS_1-B-1	3.49	80.48
TS_1-B-1 → DOL-L-PF_5-B-1	-3.86	-89.07
DOL + DOL-L-PF_5-B-1→ 2DOL-L-PF_5-B-1	-0.02	-0.45
2DOL-L-PF_5-B-1 → TS_2-B-1	0.50	11.60
TS_2-B-1 → DOL-L_2-PF_5-B-1	-0.45	-10.49

ring-opening reaction process. The energy of reactant 2DOL-L-PF_5-A is close to that of 2DOL-L-PF_5-A-1, and the energy of product DOL-L_2-PF_5-A and DOL-L_2-PF_5-A-1 is very close after the ring-opening reaction. The difference is that the energy difference of the transition state is obvious. For the second DOL ring-opening reaction, the energy of the rate-determining transition state TS_2-A is 21.19 kcal/mol in pathway I, while the highest energy of the transition state TS_2-A-1 is 55.48 kcal/mol in pathway III. Furthermore, a transition state with the lowest barrier appears in pathway IV, and the transition TS_2-B-1 energy is 11.60 kcal/mol. However, pathway II and pathway IV do not have advantages for DOL polymerization reactions in general, as they all need to go through the initial high energy transition states TS_1-B. Finally, we find that the most reasonable path of DOL polymerization is Pathway I. Meanwhile, the existing experiment supports our major predictions. For example, accumulated experimental results suggest that PF_5 is likely to initiate the polymerization, which strongly supports our prediction [27].

In experimental conditions, more reaction possibilities may exist due to the unavoidable presence of water and oxygen. We will continue to focus on more possible reactions with consideration of impurities in our further work.

Meanwhile, we are expecting experiments, such as Desorption Electrospray Ionization Mass Spectrometry (DESI), to validate our predictions.

4. Conclusions

In summary, we employed a multi-scale simulation to investigate the reaction mechanism of SEI formation on the Li metal battery in $LiPF_6$ + DOL electrolyte. Based on the simulation results, the major conclusions are as follows:

The presence of $LiPF_6$ salts in the electrolyte not only provides F^- ions for the formation of inorganic layers but also provides an initiator, the partial decomposition product of PF_5, to induce the *in situ* polymerization of DOL in forming a polymer-like organic layer. The strong interaction of PF5 with O in DOL, because of p-d π back donation, weakens the C-O bond in DOL, which induces that ring-opening reaction. The produced radical, then, propagates by reacting with other DOL to facilitate further polymerization. Finally, an SEI with the inner layer consists of a hard and dense inorganic layer and an outer layer consists of a soft and continuous organic layer is formed, which exhibits ideal balance to facilitate superior performance.

Furthermore, we disguised the most kinetically favorable reaction pathway from all four possible DOL polymerization pathways. The hybrid function calculation shows that The DOL molecular ring-opening polymerization is thermodynamically favorable with the assist of PF_5. The maximum energy

barrier in the reaction pathway is 21.19 kcal/mol, which is surmountable at room temperature. These calculation results are in good agreement with the experimental results [26, 27].

Overall, the above insights are of help to clarify the relationship between the molecular structure of electrolytes and the formation of SEI components. The understanding of the reaction mechanism of SEI formation, in turn, paves the way for the rational design of electrolytes to enhance the performance of LMBs.

Acknowledgments

T.C. and M.X. thank the National Natural Science Foundation of China (21903058 and 22003044), the Natural Science Foundation of Jiangsu Higher Education Institutions (SBK20190810), the Jiangsu Province High-Level Talents (JNHB-106), and the Priority Academic Program Development of Jiangsu Higher Education Institutions (PAPD) for financial support. WAG gratefully acknowledges support from NSF (CBET-1805022)

References

1 T. Kim, W. Song, D.-Y. Son, L. K. Ono and Y. Qi, Lithium-ion batteries: outlook on present, future, and hybridized technologies. Mater. Chem. A. 7(2019), 2942-2964.

2 M. Li, J. Lu, Z. Chen and K. Amine, 30 Years of Lithium-Ion Batteries. Adv. Mater., 30(2018), 1800561.

3 X.-B. Cheng, R. Zhang, C.-Z. Zhao and Q. Zhang, Toward Safe Lithium Metal Anode in

Rechargeable Batteries: A Review. Chem. Rev. 117(2017), 10403-10473.

4 P. Li, J.-Y. Hwang and Y.-K. Sun, Nano/Microstructured Silicon–Graphite Composite Anode for High-Energy-Density Li-Ion Battery. ACS Nano. 13(2019), 2624-2633.

5 J. Janek and W. G. Zeier, A solid future for battery development. Nat. Energy. 1(2016), 16141.

6 T. Krauskopf, F. H. Richter, W. G. Zeier and J. Janek, Physicochemical Concepts of the Lithium Metal Anode in Solid-State Batteries. Chem. Rev. 120(2020), 7745-7794.

7 Z. A. Ghazi, Z. Sun, C. Sun, F. Qi, B. An, F. Li and H.-M. Cheng, Key Aspects of Lithium Metal Anodes for Lithium Metal Batteries. Small. 15(2019), 1900687.

8 C. Niu, H. Lee, S. Chen, Q. Li, J. Du, W. Xu, J.-G. Zhang, M. S. Whittingham, J. Xiao and J. Liu, High-energy lithium metal pouch cells with limited anode swelling and long stable cycles. Nat. Energy. 4(2019), 551-559.

9 G. Wang, X. Xiong, D. Xie, X. Fu, X. Ma, Y. Li, Y. Liu, Z. Lin, C. Yang and M. Liu, Suppressing dendrite growth by a functional electrolyte additive for robust Li metal anodes. Energy. Storage. Mater. 23(2019), 701-706.

10 J. Xie and Y.-C. Lu, A retrospective on lithium-ion batteries. Nat. Commun. 11(2020), 2499.

11 X. Xu, S. Wang, H. Wang, C. Hu, Y. Jin, J. Liu and H. Yan, J. Recent progresses in the suppression method based on the growth mechanism of lithium dendrite. Energy. Chem. 27(2018), 513-527.

12 R. Zhang, N.-W. Li, X.-B. Cheng, Y.-X. Yin, Q. Zhang and Y.-G. Guo, Advanced Micro/Nanostructures for Lithium Metal Anodes. Adv. Sci. 4(2017), 1600445.

13 X. Zhang, Y. Yang and Z. Zhou, Towards practical lithium-metal anodes. Chem. Soc. Rev. 49(2020), 3040-3071.

14 H. Liu, X.-B. Cheng, J.-Q. Huang, S. Kaskel, S. Chou, H. S. Park and Q. Zhang, Alloy Anodes for Rechargeable Alkali-Metal Batteries: Progress and Challenge. ACS Mater. Lett. 1(2019), 217-229.

15 Y. Jie, X. Ren, R. Cao, W. Cai and S. Jiao, Advanced Liquid Electrolytes for Rechargeable Li Metal Batteries. Adv. Funct. Mater. 30(2020), 1910777.

16 Y. He, Y. Zhang, P. Yu, F. Ding, X. Li, Z. Wang, Z. Lv, X. Wang, Z. Liu and X. Huang, Ion association tailoring SEI composition for Li metal anode protection.J. Energy. Chem. 45(2020), 1-6.

17 C. Wang, K. Fu, S. P. Kammampata, D. W. McOwen, A. J. Samson, L. Zhang, G. T. Hitz, A. M. Nolan, E. D. Wachsman, Y. Mo, V. Thangadurai and L. Hu, Garnet-Type Solid-State Electrolytes: Materials, Interfaces, and Batteries. Chem. Rev. 120(2020), 4257-4300.

18 Q. Yang, W. Li, C. Dong, Y. Ma, Y. Yin, Q. Wu, Z. Xu, W. Ma, C. Fan and K. Sun, PIM-1 as an artificial solid electrolyte interphase for stable lithium metal anode in high-performance batteries. J. Energy. Chem. 42(2020), 83-90.

19 X.-B. Cheng, R. Zhang, C.-Z. Zhao, F. Wei, J.-G. Zhang and Q. Zhang, A Review of Solid Electrolyte Interphases on Lithium Metal Anode. Adv. Sci. 3(2016), 1500213.

20 C. Wu, F. Guo, L. Zhuang, X. Ai, F. Zhong, H. Yang and J. Qian, Mesoporous Silica Reinforced Hybrid Polymer Artificial Layer for High-Energy and Long-Cycling Lithium Metal Batteries. ACS Energy. Lett. 5(2020), 1644-1652.

21 L. Liu, Y.-X. Yin, J.-Y. Li, N.-W. Li, X.-X. Zeng, H. Ye, Y.-G. Guo and L.-J. Wan, Free-Standing Hollow Carbon Fibers as High-Capacity Containers for Stable Lithium Metal Anodes. Joule. 1(2017), 563-575.

22 F. Guo, C. Wu, S. Chen, X. Ai, F. Zhong, H. Yang and J. Qian, Flaky and Dense Lithium Deposition Enabled by a Nanoporous Copper Surface Layer on Lithium Metal Anode. ACS Mater. Lett. 2(2020), 358-366.

23 F. Ding, W. Xu, G. L. Graff, J. Zhang, M. L. Sushko, X. Chen, Y. Shao, M. H. Engelhard, Z. Nie, J. Xiao, X. Liu, P. V. Sushko, J. Liu and J.-G. Zhang, Dendrite-Free Lithium Deposition via Self-Healing Electrostatic Shield Mechanism.J. Am. Chem. Soc. 135(2013), 4450-4456.

24 J. Qian, W. A. Henderson, W. Xu, P. Bhattacharya, M. Engelhard, O. Borodin and J.-G. Zhang, High rate and stable cycling of lithium metal anode. Nat. Commun. 6(2015), 6362.

25 J. Qian, W. Xu, P. Bhattacharya, M. Engelhard, W. A. Henderson, Y. Zhang and J.-G. Zhang, Dendrite-free Li deposition using trace-amounts of water as an electrolyte additive. Nano. Energy. 15(2015), 135-144.

26 Q. Zhao, X. Liu, S. Stalin, K. Khan and L. A. Archer, A. Solid-state polymer electrolytes with in-built fast interfacial transport for secondary lithium batteries. Nat. Energy. 4(2019), 365-373.

27 F.-Q. Liu, W.-P. Wang, Y.-X. Yin, S.-F. Zhang, J.-L. Shi, L. Wang, X.-D. Zhang, Y. Zheng, J.-J. Zhou, L. Li, Y.-G. Guo, Upgrading traditional liquid electrolyte via in situ gelation for future lithium metal batteries. Sci. Adv. 4(2018) eaat5383.

28 K. Khan, Z. Tu, Q. Zhao, C. Zhao and L. A. Archer, Synthesis and Properties of Poly-Ether/Ethylene Carbonate Electrolytes with High Oxidative Stability. Chem. Mater. 31(2019), 8466-8472.

29 Y. Liu, P. Yu, Y. Wu, H. Yang, M. Xie, L. Huai, W. A. Goddard, T. Cheng, The DFT-ReaxFF Hybrid Reactive Dynamics Method with Application to the Reductive Decomposition Reaction of the TFSI and DOL Electrolyte at a Lithium‐Metal Anode Surface, J. Phys. Chem. Lett. 12(2021) 1300-1306.

30 Y. Liu, Q. Sun, P. Yu, Y. Wu, L. Xu, H. Yang, M. Xie, T. Cheng, W. A. Goddard, Effects of High and Low Salt Concentrations in Electrolytes at Lithium‐Metal Anode Surfaces Using DFT-ReaxFF Hybrid Molecular Dynamics Method, J. Phys. Chem. Lett. 2021 2922-2929.

31 G. Kresse and J. Furthmüller, Efficient iterative schemes for ab initio total-energy calculations

using a plane-wave basis set. Phys. Rev. B. 54(1996), 11169.

32 G. Kresse and J. Hafner, Ab initio molecular dynamics for liquid metals. Phys.Rev. B. 47(1993), 558-561.

33 J. P. Perdew, K. Burke and M. Ernzerhof, Generalized Gradient Approximation Made Simple. Phys. Rev. Lett. 77(1996), 3865-3868.

34 S. Grimme, J. Antony, S. Ehrlich and H. Krieg, A consistent and accurate ab initio parametrization of density functional dispersion correction (DFT-D) for the 94 elements H-Pu. J. Chem. Phys. 132(2010), 154104.

35 P. E. Blöchl, Projector augmented-wave method. Phys.Rev. B. 50(1994), 17953-17979.

36 G. Kresse and D. Joubert, From ultrasoft pseudopotentials to the projector augmented-wave method. Phys.Rev. B. 59(1999), 1758-1775.

37 N. Metropolis, A. W. Rosenbluth, M. N. Rosenbluth, A. H. Teller and E. Teller, Equation of State Calculations by Fast Computing Machines. J. Chem. Phys. 21(1953), 1087-1092.

38 S. Kirkpatrick, C. D. Gelatt and M. P. Vecchi, Optimization by Simulated Annealing. Science. 220(1983), 671-680.

39 A. D. Becke, Density□functional thermochemistry. III. The role of exact exchange. J. Chem. Phys. 98(1993), 5648-5652.

40 K. Fukui, Formulation of the reaction coordinate. J Phys Chem. 74(1970), 4161-4163.

41 K. Fukui, The path of chemical reactions - the IRC approach. Acc. Chem. Res. 14(1981), 363-368.

42 A. V. Marenich, C. J. Cramer and D. G. Truhlar, Universal Solvation Model Based on Solute Electron Density and on a Continuum Model of the Solvent Defined by the Bulk Dielectric Constant and Atomic Surface Tensions. J. Phys. Chem. B. 113(2009), 6378-6396.

43 M. J. Frisch, G. W. Trucks, H. B. Schlegel, G. E. Scuseria, M. A. Robb, J. R. Cheeseman, G. Scalmani, V. Barone, G. A. Petersson, H. Nakatsuji, X. Li, M. Caricato, A. V. Marenich, J. Bloino, B. G. Janesko, R. Gomperts, B. Mennucci, H. P. Hratchian, J. V. Ortiz, A. F. Izmaylov, J. L. Sonnenberg, D. Williams-Young, F. Ding, F. Lipparini, F. Egidi, J. Goings, B. Peng, A. Petrone, T. Henderson, D. Ranasinghe, V. G. Zakrzewski, J. Gao, N. Rega, G. Zheng, W. Liang, M. Hada, M. Ehara, K. Toyota, R. Fukuda, J. Hasegawa, M. Ishida, T. Nakajima, Y. Honda, O. Kitao, H. Nakai, T. Vreven, K. Throssell, J. A. Montgomery, Jr., J. E. Peralta, F. Ogliaro, M. J. Bearpark, J. J. Heyd, E. N. Brothers, K. N. Kudin, V. N. Staroverov, T. A. Keith, R. Kobayashi, J. Normand, K. Raghavachari, A. P. Rendell, J. C. Burant, S. S. Iyengar, J. Tomasi, M. Cossi, J. M. Millam, M. Klene, C. Adamo, R. Cammi, J. W. Ochterski, R. L. Martin, K. Morokuma, O. Farkas, J. B. Foresman, and D. J. Fox, Gaussian 16 (Revision A.03), Inc., Wallingford CT, 2016.

44 D. Chen, M. A. Mahmoud, J.-H. Wang, G. H. Waller, B. Zhao, C. Qu, M. A. El-Sayed and M. Liu,

Operando Investigation into Dynamic Evolution of Cathode–Electrolyte Interfaces in a Li-Ion Battery. Nano. Lett. 19(2019), 2037-2043.

45 S. Jurng, Z. L. Brown, J. Kim and B. L. Lucht, Effect of electrolyte on the nanostructure of the solid electrolyte interphase (SEI) and performance of lithium metal anodes. Energ. Environ. Sci. 11(2018), 2600-2608.

46 J. Ko and Y. S. Yoon, Recent progress in LiF materials for safe lithium metal anode of rechargeable batteries: Is LiF the key to commercializing Li metal batteries? Ceram. Int. 45(2019), 30-49.

47 J. Lang, Y. Long, J. Qu, X. Luo, H. Wei, K. Huang, H. Zhang, L. Qi, Q. Zhang, Z. Li and H. Wu, One-pot solution coating of high quality LiF layer to stabilize Li metal anode. Energy. Storage. Mater. 16(2019), 85-90.

48 H. Shin, J. Park, S. Han, A. M. Sastry and W. Lu, Component-/structure-dependent elasticity of solid electrolyte interphase layer in Li-ion batteries: Experimental and computational studies. J. Power. Sources. 277(2015), 169-179.

49 J. Jones, M. Anouti, M. Caillon-Caravanier, P. Willmann and D. Lemordant, Thermodynamic of LiF dissolution in alkylcarbonates and some of their mixtures with water. Fluid. Phase. Equilib. 285(2009), 62-68.

50 M. He, R. Guo, G. M. Hobold, H. Gao and B. M. Gallant, The intrinsic behavior of lithium fluoride in solid electrolyte interphases on lithium. P. Natl. Acad. Sci. USA. 117(2020), 73-79.

51 Y. Lee, T. K. Lee, S. Kim, J. Lee, Y. Ahn, K. Kim, H. Ma, G. Park, S.-M. Lee, S. K. Kwak and N.-S. Choi, Fluorine-incorporated interface enhances cycling stability of lithium metal batteries with Ni-rich NCM cathodes. Nano. Energy. 67(2020), 104309

Graphical Abstract

Description

Free radical-induced in-situ polymerization of electrolyte is beneficial to the formation of a stable inorganic-organic composite solid electrolyte interface.

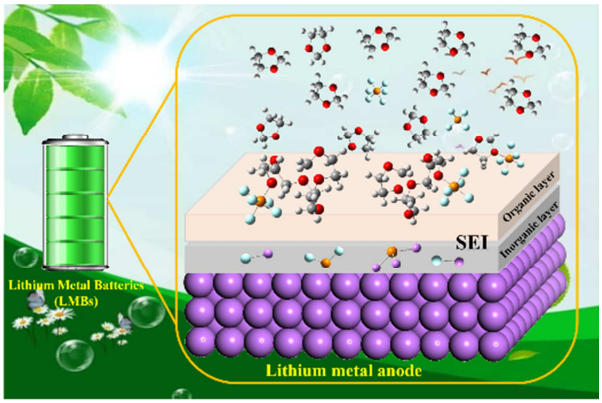

Highlights

- Polymerization of the electrolyte provides an unexpected protective effect that resembles the polymer electrolyte but is formed in situ;
- PF_5 plays an important role in activating the DOL ring for further polymerization;
- The most kinetically favorable polymerization pathway is distinguished, which provide opportunities for rational design of stable SEI by finely refining electrolyte.

Declaration of interests

☑ The authors declare that they have no known competing financial interests or personal relationships that could have appeared to influence the work reported in this paper.

☐The authors declare the following financial interests/personal relationships which may be considered as potential competing interests: